The Electrochemical Society
Advancing solid state & electrochemical science & technology

OPEN ACCESS

Degradation Phenomena in Silicon/Graphite Electrodes with Varying Silicon Content

View the article online for updates and enhancements.

You may also like

Degradation Phenomena in Silicon/Graphite Electrodes with Varying Silicon Content

Ahmad Ghamlouche,[z] Marcus Müller, Fabian Jeschull, and Julia Maibach[z]

Institute for Applied Materials, 76344 Eggenstein-Leopoldshafen, Germany

The degradation phenomena of Silicon/Graphite electrodes and the effect of FEC as electrolyte additive was investigated through galvanostatic cycling, XPS analyses and SEM cross section analyses. To understand the direct influence of silicon on the electrode degradation, the silicon amount was varied between 0%–30%. By evaluating the cycling performance and the accumulated capacity loss of the different Si/Gr electrodes (cycled with and without 10 vol-% of FEC), we see that the capacity decay can be distinguished into two phenomena, where one is independent of the Si/Gr ratio while the other one depends on the Si content. As expected, adding FEC improves the cell performance and minimizes the capacity decay. Combing our XPS data and SEM cross section analyses on cycled electrodes, this improvement stems from a thin and flexible SEI including poly(vinyl carbonate) that helps maintaining the overall electrode integrity as we observe less electrode fractures and less pronounced thickness increase. Si/Gr electrodes with 10 and 20% Si content showed very similar accumulated irreversible capacity losses over 100 cycles indicating that with 10 % FEC as electrolyte additive, also higher Si contents could be feasible for future high energy density anodes.

Adding silicon to graphite electrodes is a promising approach to increase the energy density for next generation lithium-ion batteries (LIB).[1] Compared to graphite the specific capacity of silicon is significantly higher (LiC_6, 372 mAh g^{-1}; $Li_{15}Si_4$, 3579 mAh g^{-1}).[2,3] However, the problem with silicon is the high volume change (>300%) during (de-)lithiation which leads to particle isolation,[4,5] continuous degradation of the electrolyte and ongoing formation of the solid electrolyte interphase (SEI).[6–9] These problems are responsible for the generally shorter cycle-life of silicon based electrodes compared to commonly used graphite anodes. Various approaches to overcome these problems are currently being researched that built on incorporating Si particles in a carbonaceous matrix.[10,11] One straightforward syntheses route is to mix Si nanoparticles with graphite by ball milling to create a composite electrodes.[12] Another approach to overcome the poor performance, is to use an electrolyte additive such fluoroethylene carbonate (FEC), which is known to stabilize the SEI.[13,14] FEC is widely used in Si/Gr electrodes because it significantly reduces the capacity loss and leads to improved cycling stability.[15]

In this work we evaluate in detail the influence of FEC on the degradation phenomena of Si/Gr electrodes. In the first part we discuss the electrochemical performance of Si/Gr composite electrodes with varying silicon content with and without adding FEC to the electrolyte. Secondly, X-ray photoelectron spectroscopy (XPS) and scanning electron microscopy (SEM) analyses provide a detailed view of the SEI and electrode structure. Our results show that FEC does not only influence the SEI composition but stabilizes the entire electrode by forming a stable yet flexible electrode network helping Si nanoparticles to stay electrochemically active in the composite electrodes.

Experimental

Electrode preparation.—All electrodes were prepared in an aqueous solution. A LiPAA binder was prepared by adding LiOH (Sigma-Aldrich) stepwise to a 1 wt% PAA solution (1.250.000 g mol^{-1}, Sigma-Aldrich, Germany) to a pH value of 7. Silicon particles ($\sim$ 300 nm, Wacker Chemie AG, Germany) were mixed with Graphite (MechanoCAP® 1P1, H.C. Carbon GmbH, Germany)

at ratios of 0, 10, 20, and 30% Si and vapor grown carbon fibres (VGCF, Showa Denko, Japan) were added in a Thinky Planetary Mixer and then dried for 1 h at 60 °C. The dried powders were transferred to a planetary ball mill (Pulverisette 7, Fritsch, Germany) with ZrO_2 balls (10 mm diameter) and mixed with LiPAA and 1 ml milli-pore water. The resulting slurries were cast onto copper foil using a bar coater (Coatmaster 509 MC, Erichsen, Germany). After ambient drying overnight, electrode discs of 14 mm in diameter were punched out and dried in a Büchi oven at 120 °C for 12 h under reduced pressure, before being transferred into an Ar-filled MBraun Glovebox (H_2O and O_2 concentration <0.1 ppm).

Half-cell assembly and cycling.—The electrodes were assembled in a Ar-filled glove box (Mbraun, Germany) in a coin-cell half-cell-setup with a lithium counter electrode (250 μm, Pi-Kem, United Kingdoms), one Celgard polymer (Ø 16 mm, Celgard 2325, USA) and one Whatman® glass fiber GF/A (Ø 17 mm, Sigma-Aldrich, Germany) separator. As electrolyte solution, 1 M $LiPF_6$ dissolved in a mixture of ethylene carbonate (EC) and dimethyl carbonat (DMC) (1:1 v-v, LP30, BASF; Germany) and 10 vol% fluoroethylene carbonate (FEC, BASF, Germany) was used. The cells were cycled using a multi-channel potentiostat BCS-800 (BioLogic, France) in a temperature chamber at 25 °C. The cell performances of the Si/Gr electrodes were investigated through galvanostatic cycling (constant current) with a cut off potential of 0.01 V vs Li/Li$^+$ during lithiation and 1.5 V during delithiation and with a C-Rate of C/10.

XPS.—For the XPS measurements all cycled cells were dissembled in the glovebox and washed three times with 500 μl DMC and dried at 60 °C. The measurements were performed using a K-Alpha XPS spectrometer (ThermoFisher Scientific, East Grinstead, UK). Samples were transferred between glovebox and spectrometer without exposure to air or moisture. Data acquisition and processing were done with the software Avantage (ThermoFisher Scientific). All electrodes were analyzed using a microfocused, monochromatic Al Kα X-ray source (400 μm spot size) and two different spots per electrode were measured. The spectra were fitted with one or more Voigt profiles (binding energy uncertainty: $\pm$0.2 eV). All spectra were referenced in binding energy to the C 1s peak (CC/CH) at 285.0 eV and the energy scale was controlled by the means of the well-known photoelectron peaks of metallic Cu, Ag, and Au.

[z]E-mail: ahmad.ghamlouche@kit.edu; julia.maibach@kit.edu

Electrode morphology.—Cross-sectional analyses for the pristine and cycled electrodes to investigate the electrode morphology were performed using a field-emission scanning electron microscope (Supra 55, Zeiss). The samples were cross-sectioned before inspection by ion-beam milling (EM TIC3X, Leica Microsystems) using argon ions and an accelerating voltage of 6 kV at 2.2 mA gun current.

Results

Galvanostatic cycling.—Based on the galvanic cycling results, the electrochemical (de-)lithiation potentials of Si/Gr electrodes were evaluated in differential capacity (dQ/dE vs E) plots. Figure 1 shows the differential capacity after 1 cycle at C/10 for all four electrodes. The corresponding peaks for the different lithiation stages of graphite (marked with x) can be found at 0.2 V (LiC$_{27}$), 0.1 V (LiC$_{12}$) and at 0.07 V (LiC$_6$).[16–18] All Silicon containing samples show additional features in the lithiation step which can be assigned to the alloying reaction between Li and Si (marked with *). The peak at 0.27 V is the first characteristic peak in the transition of crystalline Si to an amorphous Si-Li phase.[19,20,21] Jimenez et al. reported that the reduction peak at 0.24 V is associated with the formation of LiSi from the amorphous Si and subsequent phase transition from LiSi to Li$_7$Si$_3$.[20] A second reduction peak is clearly obtained at 0.09 V for 20% and 30% of silicon. For 10% Si, the dQ/dE curve deviates from the graphite measurement in this region and there seems to be a small shoulder. This peak is attributed to the formation of Li$_{15}$Si$_4$.[19] For 30% of silicon the peak at 0.09 V is overlapping with the graphite peak at 0.1 V (superposition).

It should be noted that the peaks for both graphite and silicon for the samples containing silicon (especially for 30%) are shifted to lower potential in the lithiation and to higher potential in the delithiation. The potential shift could be caused by the silicon which leads to an overall lower electronic conductivity and higher internal resistance in the electrode composite.[12] Additionally, for 30% Si, the

graphite in Si peaks overlap significantly in the lithiation which also causes a shift in position and increased peak width. The delithiation process shows clearly three characteristic peaks for graphite delithiation at 0.11 V, 0.15 V and 0.23 V and two peaks for silicon around 0.3 V and 0.4 V. These two peaks can be ascribed as the two-phase delithiation reaction of the crystalline phase (Li$_{15}$Si$_4$) to Li$_7$Si$_3$ and then to the amorphous LiSi phase.[20,21]

Figure 2 shows the cycling performance of the Si/Gr-electrodes with varying silicon amount for 100 cycles at C/10 without (a, b) and with 10 vol.-% of FEC (c, d). The electrodes' active material compositions and corresponding theoretical capacities are summarized in Table I. In Fig. 2a the different electrode compositions demonstrate delithiation capacities in the range of 370 mAh g^{-1} (0% silicon) to ~1300 mAh g^{-1} (30% silicon) in the first 1–5 cycles. As expected, the performance of the graphite (0% silicon) electrodes is stable over 100 cycles. The graphite columbic efficiency (CE), which is shown in Fig. 2b, is in the range of 99–100%. During the first few cycles, the Si/Gr electrodes show a similarly stable performance and high CE. However, after approximately 20 cycles, the capacity starts to decrease for all Si/Gr electrodes. The capacity decay is more severe with higher silicon amount (10% Si → 20% Si → 30% Si). This behaviour is in a good agreement with a previous work by Jeschull et al. where the authors increased the silicon amount from 5% to 20%.[22] The capacity decay of all Si/Gr electrodes continuous and after 100 cycles all Si-containing electrodes drop to the value of the Si-free electrode. It is very likely that the decay will proceed with higher cycles. As mentioned in the introduction, the volume change leads to deformation and cracks in the electrode, as well as delamination from the current collector foil. All Si-containing electrodes show a minimum in the CE (Fig. 2b) at around the 35th cycle after which the CE increases again to approx. 99% at 100 cycles. The higher the silicon content in the electrode, the more pronounced is the coulombic efficiency minimum. Wetjen et al. obtained similar results for the coulombic efficiency.[12]
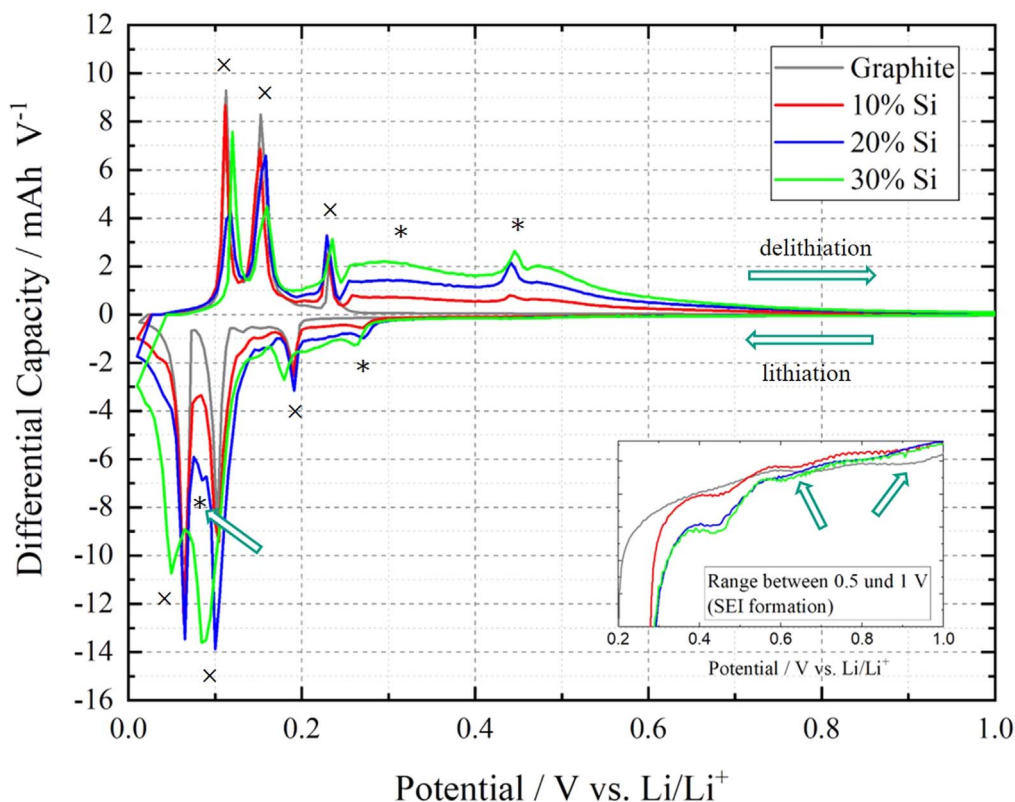

Figure 1. Differential capacity curve for Graphite, 10 wt%, 20 wt% and 30 wt% of silicon after 1 cycle. The data were obtained from the galvanostatic cycle of Si/Gr//Li coin cells with C-Rate of C/10 and LP30 as electrolyte. The inset shows the potential range of the SEI formation and the green arrows indicates the degradation peaks of the electrolyte for the graphite electrode.
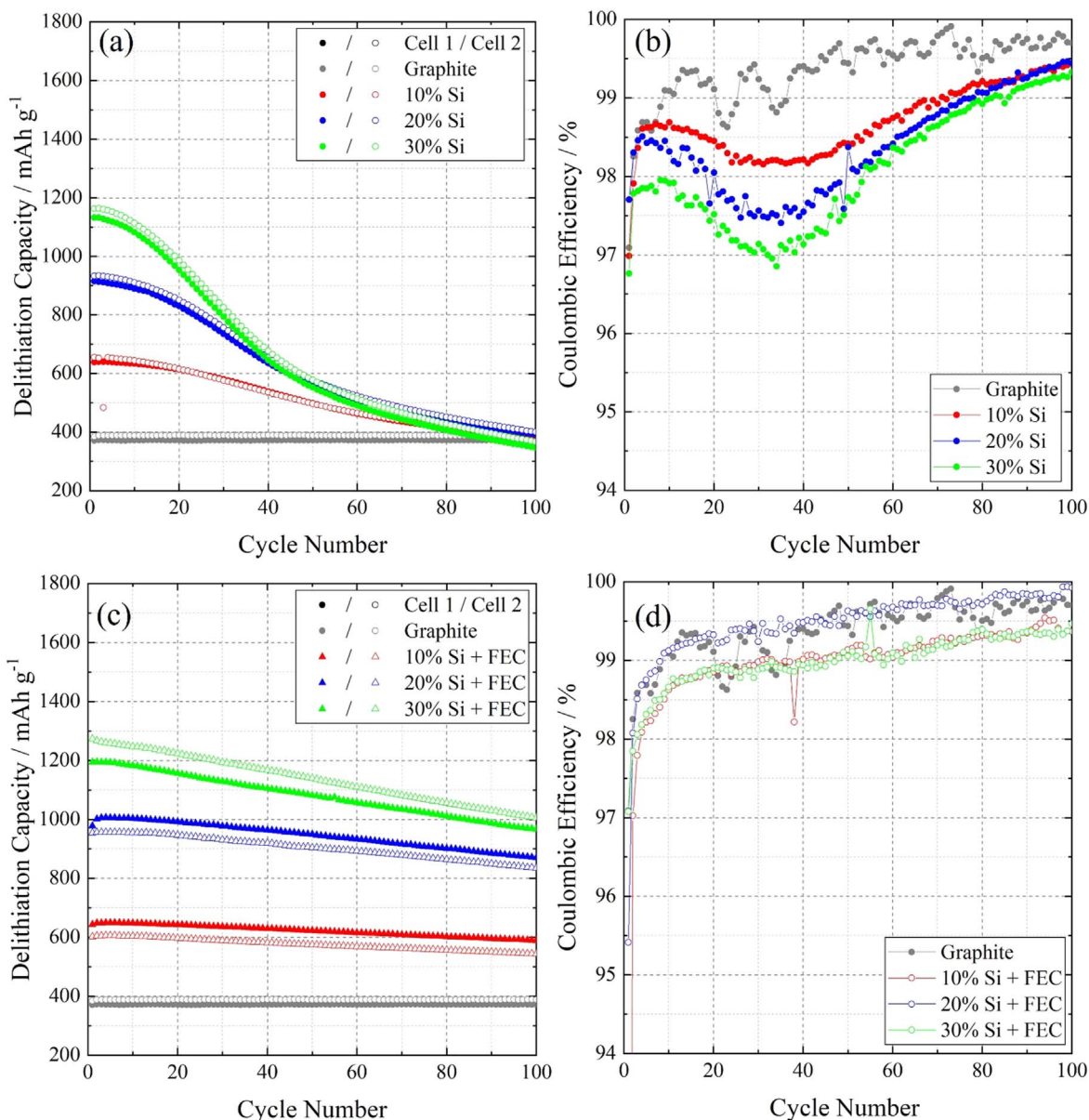
Figure 2. Galvanostatic cycling performance (C/10) of Si/Gr//Li halfcells with varying silicon amount (0–30%). (a) delithiation capacity without FEC (two identical cells for each composition), (b) coulombic efficiency plot without FEC, (c) delithiation capacity with 10% FEC (two identical cells for each composition), (d) coulombic efficiency plot with 10% FEC.

Table I. Theoretical capacities, lithiation and delithiation capacity of the first cycle and the active material compositions.

Active material composition	Si/Gr (0:100)	Si/Gr (10:90)	Si/Gr (20:80)	Si/Gr (30:70)
Theoretical capacity/mAh g^{-1}	372	692.7	1013.4	1334.1
1st Lithiation capacity/mAh g^{-1}	456	760	1080	1348
	—	778 (FEC)	1176 (FEC)	1434 (FEC)
1st Delithiation capacity/mAh g^{-1}	371	637	915	1132
	—	643 (FEC)	977 (FEC)	1193 (FEC)
CE/%	97	96	97	96
	—	97 (FEC)	95 (FEC)	97 (FEC)
Capacity retention after 100 cycle/mAh g^{-1}	371	385	391	346
	—	589 (FEC)	869 (FEC)	966 (FEC)

To investigate if and how FEC can minimize the degradation phenomena, the cells tests were repeated with a second electrolyte formulation comprising 10 vol-% of FEC. For all electrodes (except for graphite, 0 vol.-% FEC), we used the same FEC amount in the electrolyte, thus the onset of possible degradation is directly linked to the silicon amount in the electrodes. Figure 2 shows the delithiation capacity as function of cycle number (c) and the CE plot (d). As expected, the performance of the cells with 10 vol.-%

FEC is better than without FEC, however, the capacity is still decreasing. Also with FEC, it is clear that the capacity fading is more pronounced with higher silicon amount in agreement with literature.[12,22] The capacities after 100 cycles are ∼600 mAh g^{-1} (10% silicon), ∼900 mAh g^{-1} (20% silicon) and ∼1000 mAh g^{-1} (30% silicon). The CE in (d) reaches quickly over 99% and increases continuously to 99–100% after 100 cycles. Interestingly, the dip in the CE is not observed in cells operated in the FEC containing electrolyte, which is not in agreement with the results of Wetjen et al.[12] This could be due to a partly different experimental setup in this work and will be further discussed below (see Discussion).

To get a more detailed picture of the irreversible processes of Si/Gr electrodes at different stages of cycling, the accumulated capacity loss $\sum Q_{irr}$ was calculated using Eq. 1 with $Q_i^{lithiation}$ and $Q_i^{delithiation}$ as the specific lithiation and delithiation capacities in mAh g^{-1} and the index i stands for the cycle number.

$$\sum Q_{irr} = \sum_{i=1}^{100} (Q_i^{lithiation} - Q_i^{delithiation}) \qquad [1]$$

In Fig. 3 $\sum Q_{irr}$ is plotted against the cycle number for 100 cycles for the four different electrode compositions with and without 10 vol-% of FEC. $\sum Q_{irr}$ includes an initial offset for all electrodes of about ∼75–250 mAh g^{-1} corresponding to the SEI formation in the first cycle but continuously increases with cycling number indicating that some irreversible reactions take place in every cycle. The slope for all electrodes (except for graphite) is similar for the first 5 cycles whereby $\sum Q_{irr_{5th}}$ is higher with increasing silicon content (∼200 mAh g^{-1} for 10% Si; ∼300 mAh g^{-1} for 20% Si; 350 mAh g^{-1} for 30% Si). At the 10th cycle the slope for 30% Si without FEC increases more severely compared to the slope for 30% Si with FEC. Similar behaviour is obtained at the 15th cycle for 20% Si and at the 25th cycle for 10% Si. After around 40 cycles, the increase in irreversible capacity slows down for the electrodes cycled without FEC. This coincides roughly with the minimum in CE for these electrodes, which seems to indicate that the up to then dominant degradation process changes. This will be further elaborated in context of all results in the discussion section. The $\sum Q_{irr}$ also allows a more direct comparison for the 10 and 20%Si containing electrodes showing similar overall capacity losses with adding FEC.

FEC is known to decompose before EC and DMC in the used LP30 electrolyte forming a more stable SEI compared to LP30 (reduction potentials: FEC → ∼1.3 V vs Li/Li$^+$, DMC and EC → ∼ 0.5–0.8 V vs Li/Li$^+$).[12,13] The possible degradation reaction of FEC can be found in Fig. 8. Looking into Figs. 2a and 2c it seems that adding FEC does not only affect the SEI formation in the first cycles but also affects the stability of the entire electrode.

To clarify this behaviour, differential capacities for selected cycle numbers as function of the Si/Gr Potential for 20% Si with and without FEC are plotted in Fig. 4. The peak assignment follows the one presented in Fig. 1. Selected silicon peaks for lithiation and delithiation are marked with green arrows. It can be seen that the silicon peaks for the electrodes cycled without FEC get weaker from cycle to cycle and are not visible anymore after 100 cycles. For the cells cycled with FEC, the silicon peaks also decrease slightly but they are still observed after 100 cycles which agrees with the overall cycle performance. One possible reason for decreasing peak intensities when cycling without electrolyte additive is that the volume change during cycling can lead to disconnection of the silicon particles.

High resolution XPS spectra were collected after 100 cycles for all electrodes containing silicon. Figure 5 shows the C1s spectra for electrodes with10, 20 and 30% of Silicon cycled with and without FEC. All spectra are referenced in binding energy to 285 eV (CC/CH group).[15,23] All samples show an intense peak at 285 eV which can be assigned to hydrocarbon and which is a main SEI component. The
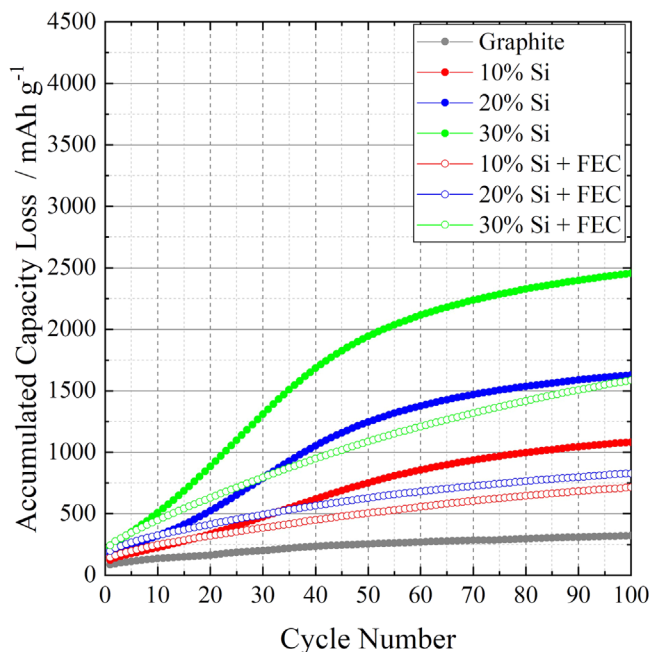

Figure 3. Accumulated Capacity Loss (defined by Eq. 1) as function of cycle number, obtained from the galvanostatic cycling data with and without 10 vol-% of FEC.

peak around 286.5 eV comes from carbon in a single bond oxygen environment.[24] Another peak at around 287.5 eV is related to a carbonyl group (C=O). In the samples with FEC (Fig. 5b) it is possible that the C=O overlaps with an additional C–F component.[7,24] Because of the similar binding energy of these species, it is not possible to sperate the peaks.[7] The peak around 289 eV belongs to a carboxylic group and at 290.2 eV to carbonate species like Li$_2$CO$_3$ and alkyl carbonates.[7,24] The cells without FEC contain slightly more carbonate species. With adding FEC an additional peak at high binding energy around 290.7 eV is observed, which can be attributed to poly(vinylene carbonate) (poly(VC)),[7,15,23,25,26] although a carbonate contribution cannot be excluded. In Fig. 5 (b) (10% Si) another peak at low binding energy around 283 eV is observed (marked with x) which can be assigned to sp^2 carbon.[7] That peak is not a SEI component but comes from graphite and the carbon fibres which are located in the bulk electrode underneath the SEI.[26] Because of the higher graphite amount for the sample with 10%Si and the effect that FEC forms a thinner SEI compared to LP30, that species is just observed for the 10% Si electrode cycled with FEC.

The O1s spectra are presented in Fig. 6. The dominant species in all samples are C=O at the binding energy around 532 eV.[15,24,25] This peak corresponds to carbonyl and carbonate groups in the C1s spectra and its slightly more pronounced in the samples without FEC. The peak at lower binding energy (∼531 eV) can be assigned to an oxygen with a carbon and lithium environment.[15,24,25] The corresponding oxygen peak for the C–O components can be found at 533 eV. For the samples with FEC another peak at high binding energy (∼534 eV) is observed and can be assigned to the poly(VC) component.[15,23,24]

SEM.—To get morphology information of the electrode, cross section scanning electron microscope (SEM) images of electrodes containing 30% of silicon are shown in Fig. 7. The pristine electrode (Fig. 7a) consists of flake-like graphite particles where nanometer-sized silicon particles are well dispersed. It can be further seen that the electrode contains free space and its partly not connected to the copper current collector. Compared to the pristine sample with the estimated coating thickness between 5 and 7 μm, the thickness of the electrode cycled without FEC (Fig. 7b) is around 13 μm after
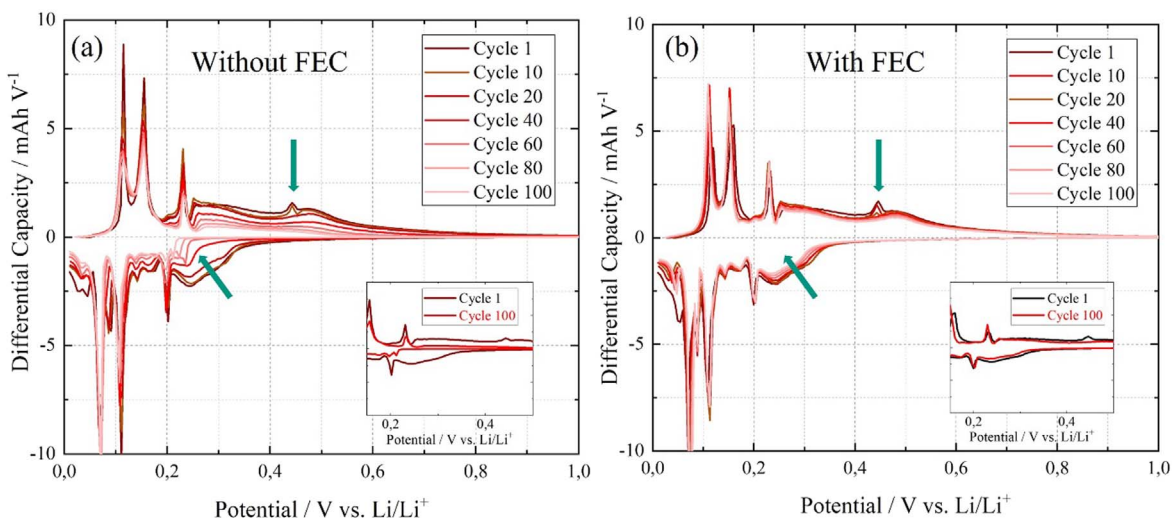
Figure 4. Differential capacity plot as function of the Si/Gr Potential vs Li/Li + for 100 cycles. (a) Si/Gr electrode with 20% Si, (b) Si/Gr electrode with 20% Si + 10 vol-% FEC.
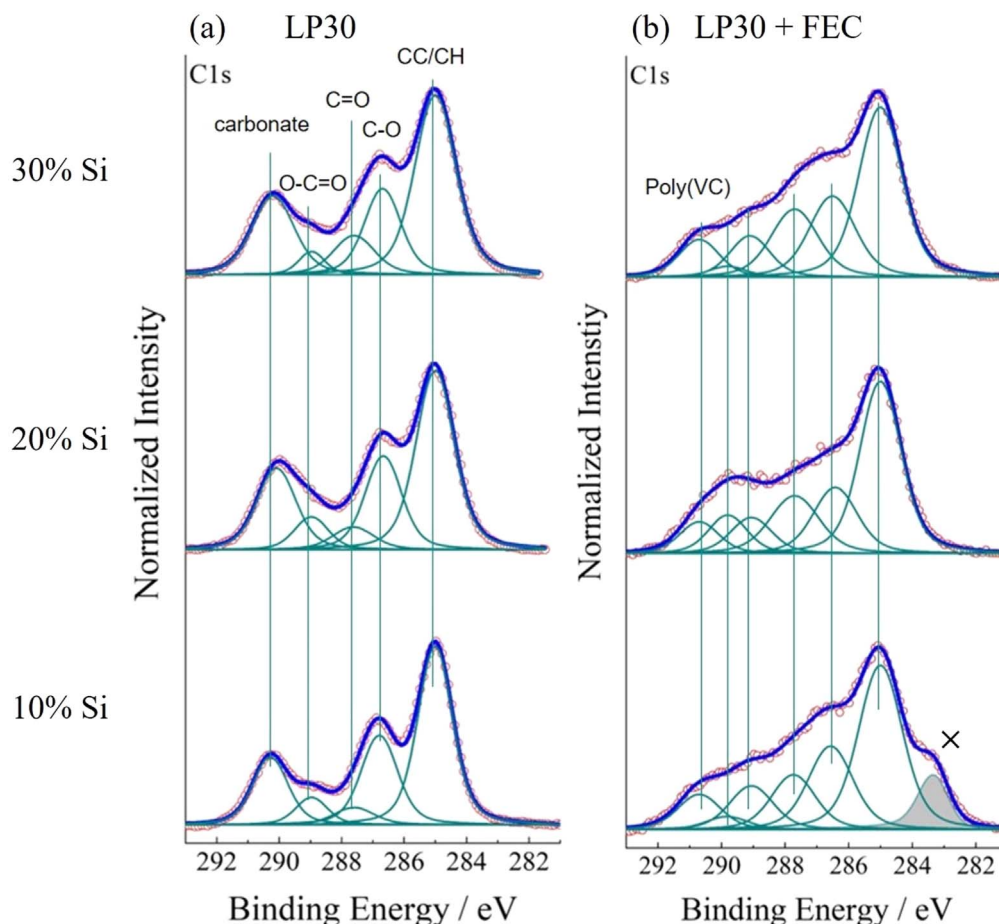

Figure 5. High resolution C1s spectra of cycled electrodes containing 10, 20, and 30% Si after 100 cycles. (a) cells without FEC, (b) cells with FEC.

cycling whereas the thickness of the electrode cylced with FEC in the electrolyte (Fig. 7c) is around 10 μm after cycling. It can be also seen that without adding FEC, bigger cracks are observed in the structure. Furthermore, the density of the electrode with FEC seems to be higher and the structure looks more compact and stable. Similar behaviours are obtained for 10 uund 20% Si and the corresponding microscopy images can be found in the supporting information (Figs. S4 and S5 (available online at stacks.iop.org/JES/169/020541/mmedia)).

Discussion

The electrochemical data presented in this work indicates two degradation mechanisms in the Si/Gr composite electrodes. All
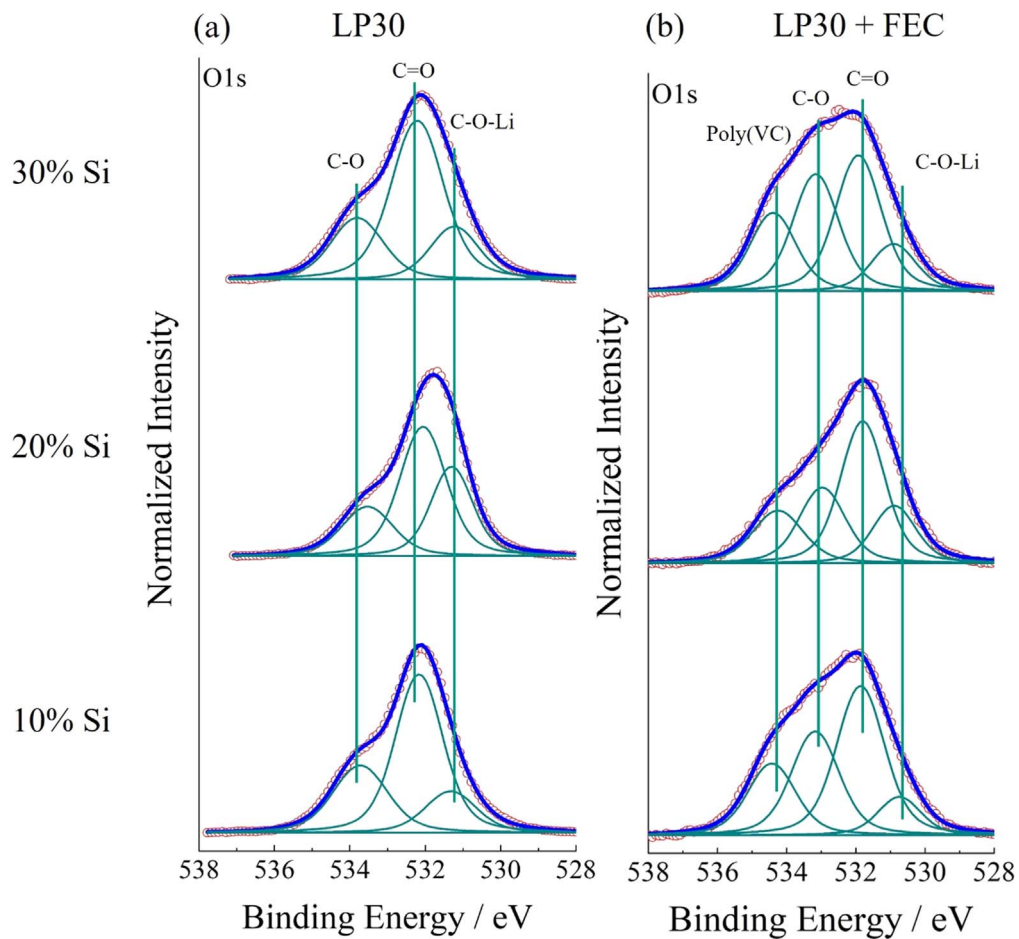
Figure 6. High resolution O1s spectra of cycled electrodes containing 10, 20 and 30% Si after 100 cycles. (a) cells without FEC, (b) cells with FEC.
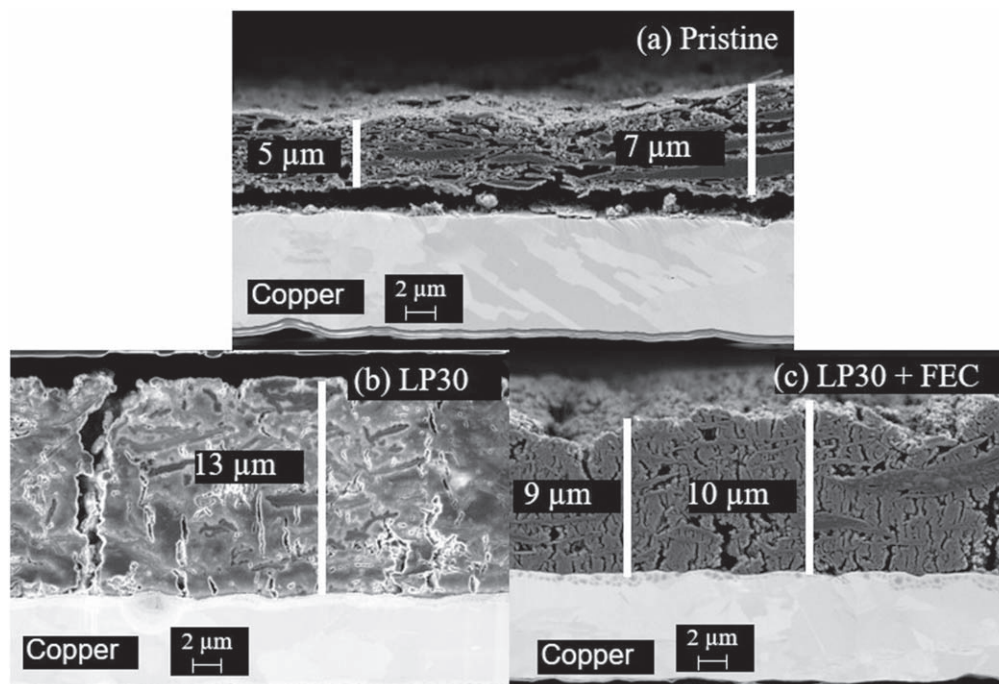

Figure 7. SEM cross section images for 30% Si. (a) Pristine electrode before cycling. (b) after 100 cycles with LP30. (c) after 100 cycles with LP30 + FEC.
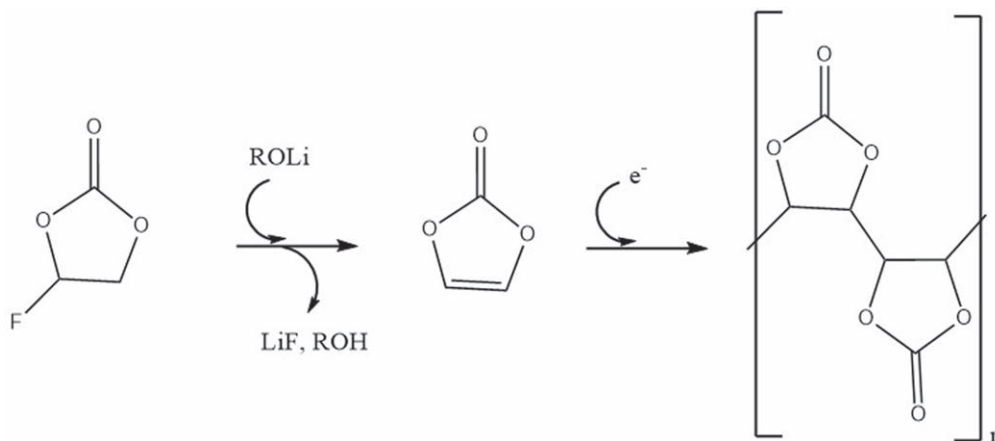
Figure 8. Possible degradation reaction of FEC to polyvinyl carbonate during electrode cycling discussed in literature.[13,25]

composite electrodes show a clear minimum in the Coulombic efficiency at approximately the same cycle number (between 30–35 cycles) when cycled without FEC in the electrolyte. The higher the Silicon content, the more pronounced is this dip and it is completely absent when only graphite is used as active material. Thus, both degradation processes are linked to silicon but only one seems to be dependent on the silicon content in the composite. The material-specific failure mechanism leading to the CE dip can be mitigated when using FEC as an electrolyte additive. But even with FEC, the electrodes with higher silicon content show more pronounced capacity decay. Similar behaviour has been observed by Wetjen et al.[12] and Jung et al.[14] where the latter described that no minimum in CE was observed for FEC contents higher than 5 vol.% in the electrolyte. In the study by Wetjen et al. it is proposed that with higher silicon content the decay of the capacity increases because of the higher mechanical stress (electrode degradation). However, their experimental setup included a varying amount of binder and conductive additive in the electrode formulation with changing Si content and a different electrolyte. In this study, we always used the same amount of binder and carbon fibres in the electrodes to get the direct influence of the silicon content on the electrode performance. Despite these experimental differences, our results are in line with the previously published data on two failure mechanisms for Si/Gr composite electrodes.

Building on this and bringing together our electrochemical data with the detailed surface and morphology analyses, we shed further light on how FEC enhances Si/Gr electrode performance. Our results indicate the FEC influences the SEI chemistry and electrode integrity. The two could be linked as one FEC decomposition pathway leads to forming elastomeric poly(VC).

Taking all presented results into account, it seems that adding FEC and the resulting forming of poly(VC) will not just produce a thinner SEI but also create a more flexibil SEI, possibly due to the eleastomeric properties of the formed poly(VC). The flexibility of the SEI also effects the stability of the whole electrode, keeping silicon electrochemically active after 100 cycles. As mentioned before, the intrinsic degradation mechanism is indepenend of the silicon amount, which can be seen in the dip in the CE plot (Fig. 2b, cells without FEC). This obtained dip is caused by the effect that the irreversible capacity loss in more pronounced in the frist 30–35 cycles. When FEC is added, no dip is obtained. Therefore FEC prevents a strong intrinsic degradation, which brings us to the hypotheses that the flexibility of poly(VC) buffers the mechanical stress to due the volume expansion and prevents particel isolation.

Conclusions

The degradation phenomena of Si/Gr electrodes with different silicon amount (0–30%) with and without adding 10 vol-% of FEC to the electrolyte have been studied. We could distinguish two different degradation phenomena of the Si/Gr electrodes. One is independent of the silicon amount, and it is due to the intrinsic properties of silicon. That can be seen in the similar coulombic efficiency drops after about 35 cycles for all electrodes containing silicon cycled in FEC-free electrolyte. On the other hand, there is a degradation mechanism which is dependent on the Si/Gr ratio as the accumulated capacity loss $\sum Q_{irr}$ increases with higher silicon amount.

By comparing the cycling behaviour of Si/Gr electrodes with three different Si-contents cycled in electrolytes without and with 10 vol-% FEC, we were able to identify, that adding FEC mostly minimizes the Si-intrinsic degradation mechanism: The minimum in the CE is not observed anymore with FEC in the electrolyte but the overall capacity fading is still more pronounced the higher the Silicon content. Based on our XPS study we could demonstrate that FEC is forming Poly(VC) resulting in a thinner SEI. This could also increase the SEI's flexibility and affects the stability of the whole electrode, keeping silicon eletrochemically active after 100 cycles. With our SEM cross section analyses we could show that the flexible SEI buffers the volume change of the silicon, which leads to a thinner electrode compared to the sample without FEC. In our setup, Si/Gr electrodes with 10 and 20% Si content showed very similar accumulated irreversible capacity losses over 100 cycles indicating that with 10 % FEC as electrolyte additive, also higher Si contents than the typically used 5%–10% could be feasible for future high energy density anodes.

ORCID

Ahmad Ghamlouche https://orcid.org/0000-0002-3345-7918
Julia Maibach https://orcid.org/0000-0003-1339-7804

References

1. S. Chae, S.-H. Choi, N. Kim, J. Sung, and J. Cho, *Angewandte Chemie (International ed. in English)*, **59**, 110 (2020).
2. M. N. Obrovac and L. Christensen, *Electrochem. Solid-State Lett.*, **7**, A93 (2004).
3. M. N. Obrovac and L. J. Krause, *J. Electrochem. Soc.*, **154**, A103 (2007).
4. B. Nguyen, J. Gaubicher, and B. Lestriez, *Electrochimica Acta*, **120**, 319 (2014).
5. C. R. Hernandez, A. Etiemble, T. Douillard, D. Mazouzi, Z. Karkar, E. Maire, D. Guyomard, B. Lestriez, and L. Roué, *Adv. Energy Mater.*, **8**, 1701787 (2018).
6. B. Philippe, R. Dedryvère, M. Gorgoi, H. Rensmo, D. Gonbeau, and K. Edström, *Chem. Mater.*, **25**, 394 (2013).

7. B. Philippe, R. Dedryvère, M. Gorgoi, H. Rensmo, D. Gonbeau, and K. Edström, *Journal of the American Chemical Society*, **135**, 9829 (2013).
8. F. Lindgren, C. Xu, J. Maibach, A. M. Andersson, M. Marcinek, L. Niedzicki, T. Gustafsson, F. Björefors, and K. Edström, *Journal of Power Sources*, **301**, 105 (2016).
9. F. Jeschull, F. Lindgren, M. J. Lacey, F. Björefors, K. Edström, and D. Brandell, *Journal of Power Sources*, **325**, 513 (2016).
10. X. Liu, X. Zhu, and D. Pan, *Royal Society open science*, **5**, 172370 (2018).
11. J.-Y. Li, Q. Xu, G. Li, Y.-X. Yin, L.-J. Wan, and Y.-G. Guo, *Mater. Chem. Front.*, **1**, 1691 (2017).
12. M. Wetjen, D. Pritzl, R. Jung, S. Solchenbach, R. Ghadimi, and H. A. Gasteiger, *J. Electrochem. Soc.*, **164**, A2840 (2017).
13. A. L. Michan, B. S. Parimalam, M. Leskes, R. N. Kerber, T. Yoon, C. P. Grey, and B. L. Lucht, *Chem. Mater.*, **28**, 8149 (2016).
14. R. Jung, M. Metzger, D. Haering, S. Solchenbach, C. Marino, N. Tsiouvaras, C. Stinner, and H. A. Gasteiger, *J. Electrochem. Soc.*, **163**, A1705 (2016).
15. V. Etacheri, O. Haik, Y. Goffer, G. A. Roberts, I. C. Stefan, R. Fasching, and D. Aurbach, *Langmuir: the ACS journal of surfaces and colloids*, **28**, 965 (2012).
16. M. Winter, J. O. Besenhard, M. E. Spahr, and P. Novák, *Adv. Mater.*, **10**, 725 (1998).
17. D. S. Moock, S. O. Steinmüller, I. D. Wessely, A. Llevot, B. Bitterer, M. A. R. Meier, S. Bräse, H. Ehrenberg, and F. Scheiba, *ACS applied materials & interfaces*, **10**, 24172 (2018).
18. W. Wang and P. N. Kumta, *Journal of Power Sources*, **172**, 650 (2007).
19. T. Azib, C. Thaury, C. Fariaut-Georges, T. Hézèque, F. Cuevas, C. Jordy, and M. Latroche, *Materials Today Communications*, **23**, 101160 (2020).
20. A. Reyes Jiménez, R. Klöpsch, R. Wagner, U. C. Rodehorst, M. Kolek, R. Nölle, M. Winter, and T. Placke, *ACS nano*, **11**, 4731 (2017).
21. M. Klett, J. A. Gilbert, S. E. Trask, B. J. Polzin, A. N. Jansen, D. W. Dees, and D. P. Abraham, *J. Electrochem. Soc.*, **163**, A875 (2016).
22. F. Jeschull, Y. Surace, S. Zürcher, M. E. Spahr, P. Novák, and S. Trabesinger, *Electrochimica Acta*, **320**, 134602 (2019).
23. S. Dalavi, P. Guduru, and B. L. Lucht, *J. Electrochem. Soc.*, **159**, A642 (2012).
24. T. Kennedy, M. Brandon, F. Laffir, and K. M. Ryan, *Journal of Power Sources*, **359**, 601 (2017).
25. V. Winkler, T. Hanemann, and M. Bruns, *Surf. Interface Anal.*, **49**, 361 (2017).
26. C. Xu, F. Lindgren, B. Philippe, M. Gorgoi, F. Björefors, K. Edström, and T. Gustafsson, *Chem. Mater.*, **27**, 2591 (2015).